Talanta 278 (2024) 126516

Contents lists available at ScienceDirect

Talanta

journal homepage: www.elsevier.com/locate/talanta

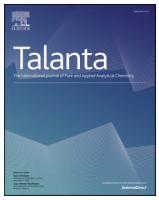

A ratiometric fluorescence sensor for detection of organophosphorus pesticides based on enzyme-regulated multifunctional Fe-based metal-organic framework

Cheng-Lin Yang, Li-Hong Yu, Yue-Hong Pang, Xiao-Fang Shen *

School of Food Science and Technology, Jiangnan University, Wuxi, 214122, China

ARTICLE INFO

Keywords:
Organophosphorus pesticides
Nanozyme
Metal-organic framework
Ratiometric fluorescence
Enzyme-based inhibition

ABSTRACT

The residues of organophosphorus pesticides (OPs) are increasing environmental pollution and public health concerns. Thus, the development of simple, convenient and sensitive method for detection of OPs is crucial. Herein, a multifunctional Fe-based MOF with fluorescence, catalytic and adsorption, is synthesized by a simple one-pot hydrothermal method. The ratiometric fluorescence sensor for detection of OPs is constructed by using only one multifunctional sensing material. The NH_2-MIL-101(Fe) is able catalyze the *o*-phenylenediamine (OPD) into 2,3-diaminophenazine (DAP) in the presence of H_2O_2. The generated DAP can significantly quench the intrinsic fluorescence of NH_2-MIL-101(Fe) by the fluorescence resonance energy transfer (FRET) and internal filtration effect (IFE), while producing a new measurable fluorescence. Without immobilization or molecular imprinting, pyrophosphate ion (PPi) can inhibit the peroxidase-like activity of the NH_2-MIL-101(Fe) by chelating with Fe^{3+}/Fe^{2+} redox couple. Moreover, PPi can also be hydrolyzed by alkaline phosphatase (ALP), the presence of OPs inhibits the activity of ALP, resulting in the increase of extra PPi preservation and signal changes of ratiometric fluorescence, the interactions of ALP with different OPs are explored by molecular docking, the OPs (e.g., glyphosate) interact with crucial amino acid residues (Asp, Ser, Ala, Lys and Arg) are indicated. The proposed sensor exhibits excellent detection performance for OPs with the detection limit of 18.7 nM, which provides a promising strategy for detection of OPs.

1. Introduction

In the last decades, organophosphate pesticides (OPs) are widely applied in agricultural production for protecting crops and maintaining yield of agricultural crops [1]. However, indiscriminate use of OPs may easily cause the pollution of water, soil and agricultural products, posing serious threats to environment and human health [2,3]. Therefore, the development of a simple, reliable and highly sensitive OPs detection method is of great significance for maintaining ecological environment and public health. Thus far, a number of methods for detection of OPs have been developed such as gas chromatography (GC), gas chromatography-mass spectrometry (GC-MS), high-performance liquid chromatography (HPLC), enzyme-linked immunosorbent assay (ELISA) [4–7]. These methods are precise and sensitive, but the economic factors restrict them not widely available for detection of OPs in the resource-limited regions of the world [8].

In recent years, fluorescence detection has been widely proposed for its simple operation, high sensitivity, visual result reading and relatively low cost [9–11]. Particularly, ratiometric fluorescence sensors based on the ratio of two independent signals are well suited for the detection of hazardous substances, which can overcome external environment interference and broaden linear range due to their built-in calibrations [12,13]. Xie et al. [14] constructed a ratiometric fluorescence sensor for detection of chlorpyrifos based on the peroxidase-like activity of MnO_2 nanosheets and fluorescence properties of near-infrared carbon dots. Yan et al. [15] used silica sphere for trapping different CdTe quantum dots and developed a ratiometric fluorescent method for detection of parathion-methyl. In the classical construction strategy of ratiometric fluorescence sensor, the researchers often focused on finding two fluorescent materials with different emission peaks or preparing two materials to perform different functions such as luminescence and catalysis [16–18], this is inevitably accompanied by more synthesis steps and variables of detection. Hence, it is still necessary to use less sensing materials to construct ratiometric fluorescence sensor for sensitive

* Corresponding author.
E-mail address: xfshen@jiangnan.edu.cn (X.-F. Shen).

https://doi.org/10.1016/j.talanta.2024.126516
Received 30 March 2024; Received in revised form 31 May 2024; Accepted 3 July 2024
Available online 4 July 2024

detection of OPs.

Metal organic frameworks (MOFs) are assembled by organic linkers and metal ions or clusters [19]. Functional MOFs can be rationally designed by changing various metal ions and organic ligands or optimizing the synthesis conditions, which are used in the catalysis, energy storage, gas adsorption, sensing and other fields [20–22]. Recently, fluorescence sensors based on luminescent MOFs and colorimetric sensors based on MOFs with biomimetic catalytic activity have attracted increasing interest in the field of analytical chemistry. Yuan et al. [23] used UiO-66-NH_2/MnO_2 fluorescence probe to detect the OPs. Wang et al. [24] constructed a colorimetric sensor based on peroxidase-mimicking Zr-MOF for the determination of phosphorylated proteins. Although the purpose of analysis could be realized by a single function of MOFs, multifunctional MOFs probe can avoid the additional cost of fluorescent dyes, multiple materials synthesis and manufacturing process of composite materials. However, as far as we know, there is still limited research on multifunctional MOFs probe for detection of hazardous substance based on rational designed. Therefore, it is of great significance to develop the ratiometric fluorescence sensor based on multifunctional MOFs and further study sensing mechanism in the biosensing fields.

In this study, multifunctional Fe-based MOF was fabricated via a simple one-pot hydrothermal method. The enzyme-mimicking property, photoluminescence property and interactions with pyrophosphate ion (PPi) of the NH_2-MIL-101(Fe) were systematically discussed. A rapid, convenient and sensitive ratiometric fluorescence method for detection of OPs was developed based on enzyme-regulated multifunctional NH_2-MIL-101(Fe). Moreover, the inhibitory process of OPs (e.g., glyphosate) for alkaline phosphatase (ALP) has been revealed through molecular simulation technology, the interactions of glyphosate with crucial amino acid residues (Asp, Ser, Ala, Lys and Arg) were indicated. The proposed sensor could achieve ratiometric fluorescence sensing based on employing only one multifunctional sensing material, which avoided the additional cost of multiple materials synthesis, thus providing a novel strategy for the detection of OPs in the food and environment samples.

2. Experiment

2.1. Chemicals and reagents

All chemicals and reagents were of analytical grade or higher. N, *N*-dimethylformamide (DMF), tris(hydroxymethyl)-aminomethane (Tris), hydrochloric acid, NaOH, NaCl, KCl, $MgCl_2$, $CaCl_2$, Na_2CO_3, $NaNO_3$, Na_2SO_4, $FeCl_3{\cdot}6H_2O$, ethanol absolute, glucose, acetic acid, citric acid, oxalic acid, dichloromethane, 30 % hydrogen peroxide and sodium pyrophosphate were obtained from Sinopharm Chemical Reagent Co., ltd. (Shanghai, China). 2,2′-Azinobis-(3-ethylbenzthiazoline-6-sulphonate) (ABTS), 3,3′,5,5′-Tetramethylbenzidine (TMB), 2-Aminoterephthalic Acid (NH_2-BDC), various types of OPs and other types of pesticides purchased from Aladdin Biochemical Technology Co., ltd (Shanghai, China). ALP was provided by Sigma-Aldrich, China. 1,2-diaminobenzene (OPD) was obtained from Macklin Biochemical Technology Co., ltd. (Shanghai, China). The water was ultrapure water purchased from Wahaha Group Co., ltd. (Hangzhou, China).

2.2. Preparation of NH_2-MIL-101(Fe)

NH_2-MIL-101(Fe) was synthesized by the hydrothermal reaction strategy, according to previous reports with slight modifications [25]. Briefly, the NH_2-BDC powder with mass of 0.725 g was dissolved in 16 mL DMF to get the monomer solution and the $FeCl_3{\cdot}6H_2O$ with mass of 1.082 g was dissolved in 24 mL DMF to make solutions of the metal ions. Above two solutions were sonicated for 5 min ensuring that the solid was completely dispersed. Then, two solutions were mixed and 4 mL of acetic acid was added. The obtained mixture was transferred into a high-pressure reaction kettle heated with polytetrafluoroethylene lining at 120 °C for 12 h. After the reaction, the reaction kettle was cooled down to room temperature in fume hood, then the precipitate was collected by centrifugation (10000 r/min, 5 min). After that, the precipitate was washed with ethyl alcohol and DMF, and dried at 60 °C for 12 h under vacuum to get reddish brown precipitate.

2.3. Investigation of fluorescence response and peroxidase-like activity

In a typical experiment, 1.98 mL acetic acid buffer solution (0.1 M pH 5.0) and 20 μL NH_2-MIL-101(Fe) aqueous suspension (1 mg/mL) were added to a 5 mL centrifuge, and the mixture was shaken. Then, the fluorescence excitation and emission spectra were recorded with a fluorescence spectrometer (Hitachi F-7000, Japan).

The peroxidase-like activity of NH_2-MIL-101(Fe) was evaluated by performing a model experiment, OPD was chosen as a typical chromogenic substrate. 1.92 mL acetic acid buffer solution (0.1 M pH 5.0), H_2O_2 (30 μL, 1 M) solution, OPD (30 μL, 0.1 M) and 20 μL NH_2-MIL-101(Fe) aqueous suspension (1 mg/mL) were added to a 5 mL centrifuge and incubated for 15 min, and the mixture was shaken. Then, the absorbance at 450 nm of the mixture was recorded and the fluorescence emission spectra was measured at an excitation wavelength of 380 nm.

2.4. Measurement procedures of glyphosate

Glyphosate was chosen as model OPs. Various concentrations of glyphosate were mixed with ALP (100 μL, 2.5 mg/L) in 5 mL centrifuge tubes and incubated at 37 °C for 30 min. Then, 100 μL solution of 80 μM PPi and Tris-HCl (50 mM, pH 10.0) were added and incubated again at 37 °C for 60 min. After that, 1.52 mL acetic acid buffer solution (0.1 M pH 5.0), H_2O_2 (30 μL, 1 M) solution, OPD (30 μL, 0.1 M) and 20 μL NH_2-MIL-101(Fe) aqueous suspension (1 mg/mL) were added to the resulted solution and incubated at room temperature for 15 min. Lastly, the fluorescence emission spectra were immediately measured.

The anti-interference experiment was performed as described above. Differently, replacing glyphosate with various ions and compounds.

2.5. Detection of real samples

Food and environmental samples were tested for a spiked recycling experiment. Each sample was spiked with glyphosate (0 μM, 0.5 μM and 2.5 μM) and measured three times. Detailed procedures of sample pretreatment were described in the supplementary materials.

3. Results and discussion

3.1. Construction of ratiometric fluorescence sensor based on multifunctional NH_2-MIL-101(Fe) for OPs assay

The OPs could exert irreversible inhibitory effect on ALP activity, the ratiometric fluorescence sensing of OPs was achieved by monitoring the activity of ALP. As shown in Scheme 1, the NH_2-MIL-101(Fe) had an intrinsic blue fluorescence at 440 nm ($\boldsymbol{F_{440}}$) and could be used as a fluorescent indicator. Meanwhile, it could also be used as a nanozyme with peroxidase-like activity. In the presence of H_2O_2, the OPD could be oxidized by NH_2-MIL-101(Fe) to generate DAP, which could produce a new fluorescence emission peak at 570 nm ($\boldsymbol{F_{570}}$) under the same excitation wavelength (λ_{ex} = 380 nm) and quench the intrinsic fluorescence signal of NH_2-MIL-101(Fe). Interestingly, PPi could specifically bind to central metal Fe and inhibit the peroxidase-like activity of NH_2-MIL-101 (Fe), thus reducing production of DAP and changing the fluorescence signaling output. Moreover, PPi could be hydrolyzed to by ALP, which implied the enzyme activity of ALP could be monitored by fluorescence signal change. The presence of OPs decreased ALP activity and increased PPi content, which caused ratiometric fluorescence signal $\boldsymbol{F_{440}/F_{570}}$ enhancement, thus sensitive detection of OPs was achieved. The practical applications of the ratiometric fluorescence sensor were verified by

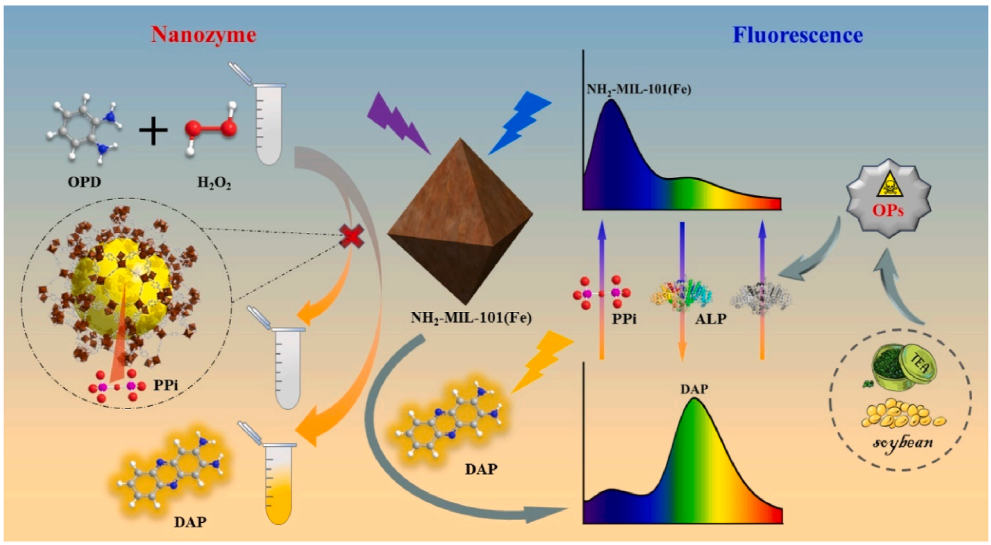

Scheme 1. Principle of ratiometric fluorescence sensing for OPs detection based on the multifunctional NH_2-MIL-101(Fe).

recording the recovery rate in the water, soil, tea and soybean samples.

3.2. Characterization of NH_2-MIL-101(Fe)

As shown in Fig. 1A and Fig. S1, the prepared NH_2-MIL-101(Fe) has the octahedral structure, and the size distribution was in the range of 100–300 nm. The XRD patterns displayed the main characteristic diffraction peaks of the NH_2-MIL-101(Fe) at around $2\theta = 9.20°$, 10.28° and 16.62° were agreeable with the XRD diffraction pattern of simulated MIL-101 (Fig. 1B), indicating the as-synthesized NH_2-MIL-101(Fe) had a pure MOFs phase [26]. The FT-IR spectrum was used to study the chemical structure of NH_2-MIL-101(Fe) (Fig. 1C). The band at 770 cm^{-1} was attributed to C–H stretching vibration in the benzene ring [27]. Due to the organic ligand (NH_2-BDC) had carboxyl group, NH_2-MIL-101(Fe) exhibited C═O asymmetric stretching vibration at 1431 cm^{-1} and C–O symmetric stretching vibration at 1573 cm^{-1} [28]. The peak at 1656 cm^{-1} corresponded to the amide group from DMF [26]. Moreover, the peaks at 3464 cm^{-1} and 3366 cm^{-1} could be assigned to the asymmetric and symmetric amines stretching [29], respectively. Corresponding to the FT-IR spectrum of NH_2-BDC, indicating the successful introduction of NH_2-BDC in NH_2-MIL-101(Fe).

The XPS spectrum of NH_2-MIL-101(Fe) showed the existence of Fe (3.59 %), O (27.00 %), N (6.22 %) and C (63.19 %) elements (Fig. 1D). The spectrum of Fe 2p was composed of two spin-orbit doublets, Fe $2p_{1/2}$ with binding energy of 725.0 eV and Fe $2p_{3/2}$ with binding energy of 711.2 eV, which could be ascribed to both Fe^{3+} and Fe^{2+} (Fig. 1E) [30]. The Fe^{3+}/Fe^{2+} redox couple was potential active sites, which played important roles in the catalytic reaction of NH_2-MIL-101(Fe) [31]. The N 1s spectrum could be split into two peaks at 400.1 eV and 398.7 eV, belonging to N–C═O and C–N/N–H, respectively (Fig. 1F). This indicated that the presence of amino group [32].

3.3. Fluorescence response and peroxidase-like activity of NH_2-MIL-101 (Fe)

The NH_2-MIL-101(Fe) with NH_2-BDC as organic ligand has been regarded as photoluminescence. In order to test this hypothesis, fluorescence spectra of NH_2-MIL-101(Fe) was registered in 0.1 M acetate buffer solution at pH = 5.0. As shown in Fig. 2A, the fluorescence spectra displayed two broad bands (excitation band at 200–400 nm and emission band at 400–530 nm), with peaks at 337 nm and 440 nm, respectively. In addition, under irradiation with a UV lamp at 365 nm, blue fluorescence of the NH_2-MIL-101(Fe) solution was clearly observed. The results confirmed that NH_2-MIL-101(Fe) could be used as a fluorescent indicator for OPs detection.

To investigate the peroxidase-like activity of NH_2-MIL-101(Fe), it was used for the catalysis of chromogenic substrates. As shown in Fig. 2B, upon addition of H_2O_2 and OPD in acetate buffer systems (0.1 M pH 5.0), the NH_2-MIL-101(Fe) could oxidize OPD to generate yellow colored DAP and the characteristic absorption peak in the vicinity of 450 nm. Similarly, other chromogenic substrates could also be catalyzed by NH_2-MIL-101(Fe), thus generating different absorption peaks and color reactions. The results demonstrated that NH_2-MIL-101(Fe) has intrinsic peroxidase-like activity, due to the presence of Fe^{3+}/Fe^{2+} redox couple. To gain further insights on the peroxidase-like activity of NH_2-MIL-101(Fe), the steady-state kinetic parameters for NH_2-MIL-101(Fe) were examined (Figs. S2A and S2C), as the concentration of substrates (TMB and H_2O_2) increased, the reaction rate gradually increased and tended to approach the maximum value. This was consistent with the Michaelis-Menten kinetic model [33,34]. The kinetic parameters were obtained using Lineweaver–Burk plots of the double reciprocal of the Michaelis–Menten equation (Figs. S2B and S2D), the K_m values of NH_2-MIL-101(Fe) for TMB and H_2O_2 were 0.32 mM and 5.41 mM, respectively. The K_m value of TMB was lower than the 0.434 mM of horseradish peroxidase [35], indicating that the as-synthesized NH_2-MIL-101 (Fe) has a higher affinity for TMB than HRP. In addition, compared to the freshly prepared NH_2-MIL-101(Fe), the fluorescence response and peroxidase-like activity of the NH_2-MIL-101(Fe) showed no signs of changes during storage of half of a year in desiccator at room temperature (Fig. S3), the NH_2-MIL-101(Fe) showed excellent chemical stability at room temperature.

The fluorescence emission peak of NH_2-MIL-101(Fe) and the UV–vis absorption peak of DAP were observed to have significant overlap (Fig. 2C). The results indicated that the fluorescence quenching mechanism of NH_2-MIL-101(Fe) caused by DAP could be attributed to the occurrence of fluorescence resonance energy transfer (FRET) or internal filtration effect (IFE) [36]. IFE and FRET could be distinguished by studying the fluorescence lifetime of donor molecule [37]. As shown in Fig. 2D, the DAP caused the fluorescence lifetime of NH_2-MIL-101(Fe) to decay from 14.06 ns to 9.57 ns, which indicated that the occurrence of FRET effect between NH_2-MIL-101(Fe) and DAP. Meanwhile NH_2-MIL-101(Fe) and DAP serve as the energy donor and acceptor in the FRET process, respectively. According to equation (**Eq. S1**), the FRET efficiency E_1 was calculated to be 31.9 % based on the fluorescence lifetime, while according to equation (**Eq. S2**), the fluorescence quenching efficiency E_2 of NH_2-MIL-101 (Fe) was 58.1 %. E_1 was lower

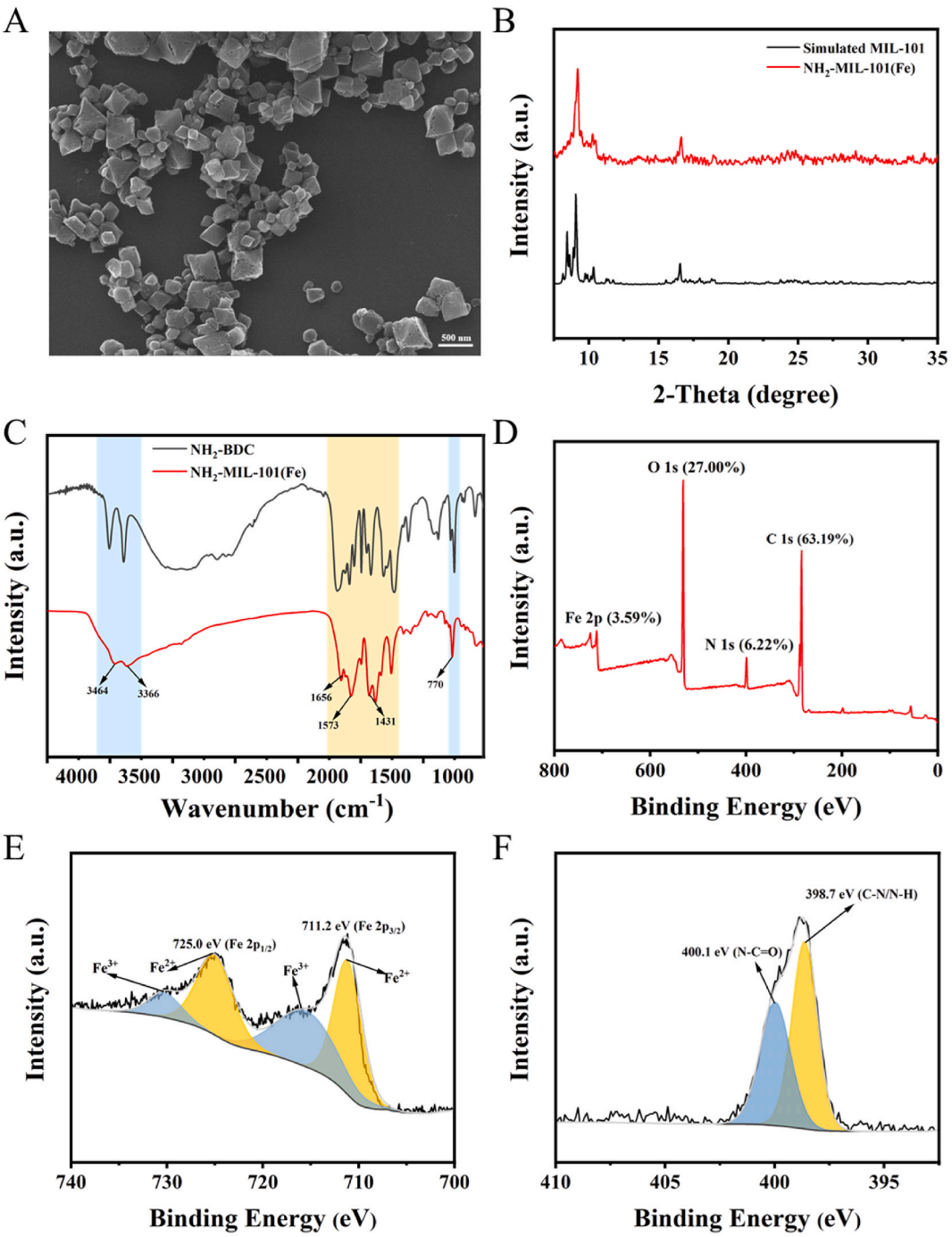

Fig. 1. (A) SEM micrograph of the NH_2-MIL-101(Fe). (B) The XRD patterns of NH_2-MIL-101(Fe) and simulated MIL-101. (C) FT-IR spectrum of NH_2-BDC and NH_2-MIL-101(Fe). (D) The XPS spectrum of NH_2-MIL-101(Fe), (E) Fe 2p, (F) N 1s.

than E_2, indicating that the FRET effect might not be the only pathway involved in the fluorescence quenching process of NH_2-MIL-101 (Fe), it may also be accompanied by the occurrence of IFE [38].

3.4. Principle of ratiometric fluorescence sensing strategy

The ratiometric fluorescence sensor for OPs detection could be constructed by coupling the NH_2-MIL-101(Fe)/OPD system with PPi. As shown in Fig. 3A, NH_2-MIL-101(Fe) exhibited a fluorescence emission peak of 440 nm at excitation wavelength of 380 nm, which was attributed to the presence of the organic ligand NH_2-BDC. There were no fluorescence signal in the solution systems of OPD, H_2O_2, and OPD + H_2O_2. However, when NH_2-MIL-101(Fe) was added to the OPD + H_2O_2 solution system, the fluorescence emission peak of NH_2-MIL-101(Fe) significantly decreased at 440 nm and a new fluorescence emission peak appeared at 570 nm. When PPi was added to the NH_2-MIL-101(Fe)/OPD/H_2O_2 catalytic system, PPi would chelate with iron metal nodes in NH_2-MIL-101(Fe) through Fe–O bond, resulting in the peroxidase-like activity of NH_2-MIL-101(Fe) was inhibited significantly, the fluorescence of the system showed the fluorescence intensity of DAP decreased while that of NH_2-MIL-101(Fe) increased. Insets were photographs of the samples from each solution systems. The intensity of the yellow color could be roughly used to determine the production of DAP.

ALP could hydrolyze PPi by breaking phosphodiester (phosphorus-

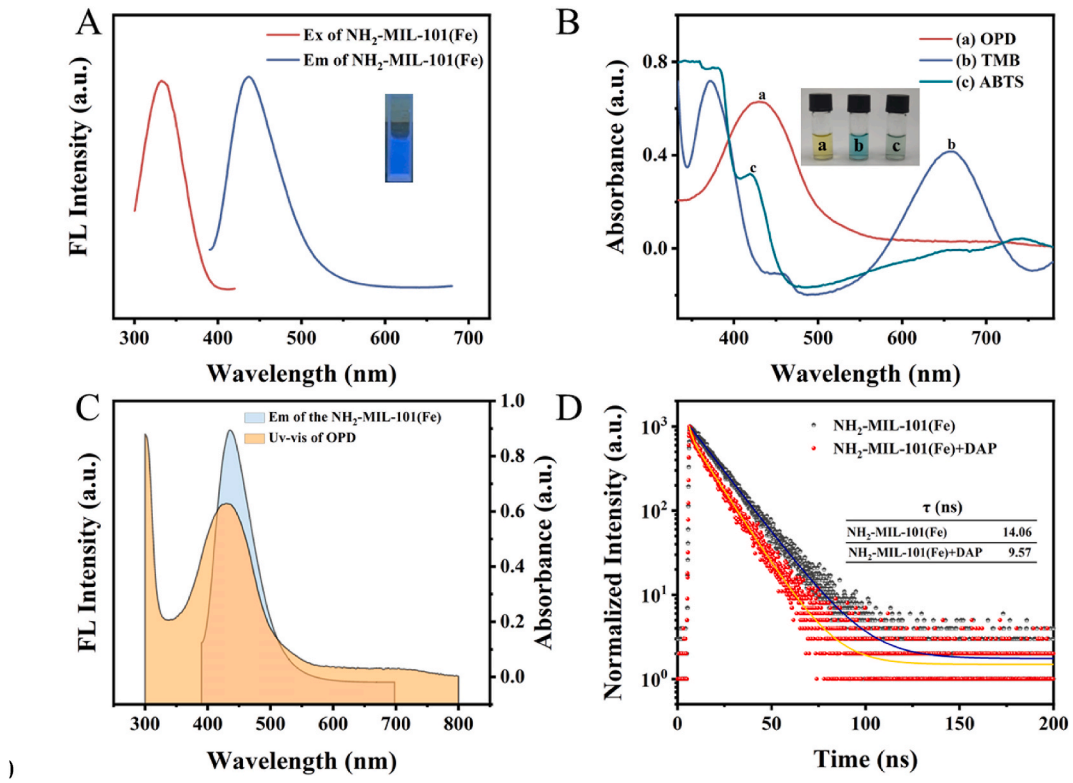

Fig. 2. (A) Fluorescence excitation, and emission spectra of NH_2-MIL-101(Fe) (Inset: photographs of NH_2-MIL-101(Fe) solution under daylight and UV light at 365 nm). (B) The UV–vis absorption spectra of different chromogenic substrates with NH_2-MIL-101(Fe) (Insets: the corresponding photos taken under white light conditions). (C) UV–vis absorption spectra of DAP and the fluorescence emission spectra of NH_2-MIL-101(Fe). (D) Fluorescence lifetimes of the NH_2-MIL-101(Fe) in the absence and presence of DAP.

oxygen) bond in PPi [39]. When ALP was added to the NH_2-MIL-101 (Fe)/OPD/H_2O_2/PPi system could restore the peroxidase-like activity NH_2-MIL-101(Fe), the fluorescence of the system showed the F_{570} increased and F_{440} decreased (Fig. 3B). The addition OPs significantly decreased the activity of ALP, the fluorescence system would retain more PPi. This change again promoted the inhibition of PPi for peroxidase-like activity NH_2-MIL-101(Fe), the fluorescence of the system showed F_{570} decreased while that F_{440} increased. These fluorescence changes effectively verify the feasibility of using NH_2-MIL-101(Fe) to detection OPs in ratiometric fluorescence sensing mode.

In order to study the interaction between NH_2-MIL-101(Fe) and PPi to clarify the sensing mechanism, the UV–vis absorption spectrum of NH_2-BDC and PPi were tested (Fig. S4). After addition of PPi, the absorption peak of NH_2-BDC had a blue-shifted. This was attributed to the electrostatic interaction between NH_2-BDC and PPi with the formation of hydrogen bonds, which leaded to PPi more easily to bind to the NH_2-MIL-101(Fe) surface. As shown in Figs. S5A and S5B, the NH_2-MIL-101 (Fe) exhibited type I and type V adsorption/desorption behavior, which was ascribed to the existence of the mesoporous and microporous structure [40]. The NH_2-MIL-101(Fe) with 0.26 cm^3/g porosity has a high surface area, which could provide a wealth of adsorptive and catalytic sites. The maximum diameter of the PPi molecular was 7.86 Å (Fig. S5C), the size of PPi was similar to half the average pore diameter of the NH_2-MIL-101(Fe), indicating that PPi was easily adsorbed by the NH_2-MIL-101(Fe).

The PPi has a strong ability to chelate with iron ions due to its presence of two phosphate groups [41]. In order to verify the binding interaction between PPi and central metal Fe, the narrow range O 1s XPS spectra of the NH_2-MIL-101(Fe) before and after the addition of PPi were also recorded. As shown in Fig. 3C, the peak of O 1s can be deconvoluted into three peaks, the peak at 530.58 eV was typical of metal-oxygen bonds, the peak at 531.38 eV was related to the oxygen component on the carboxyl, the binding energy peak at 532.68 eV was attributed to the C–O band [38]. Similar peaks were observed after addition of PPi (Fig. 3D). Remarkably, the peak of Fe–O slightly decreased, a new weak peak appeared at 535.38 eV and speculated it might attribute to the P–O band, indicating that PPi could chelate with Fe^{3+} or Fe^{2+} in NH_2-MIL-101(Fe), thereby preventing electron transfer between Fe^{3+}/Fe^{2+} redox couple and leading to a decrease in the peroxidase-like activity of NH_2-MIL-101(Fe).

3.5. Optimization of experimental conditions

To improve sensing performance of the proposed sensor for OPs detection, the main experimental parameters including the pH, time and addition concentration (OPD, H_2O_2, AAP and ALP) were investigated. As shown in Fig. S6A, DAP exhibited the highest fluorescence quenching efficiency for NH_2-MIL-101(Fe) at pH 5.0. The incubation time of the ALP with the OPs was 40 min, OPs displayed maximum inhibition rate on ALP (Fig. S6B). When the concentrations of OPD and H_2O_2 were at 2 mM and 20 mM, respectively, the catalytic efficiency of NH_2-MIL-101 (Fe) tended to reach equilibrium (Figs. S6C and S6D). The concentration of PPi was 4 μM could precisely inhibit peroxidase-like activity of NH_2-MIL-101(Fe) (Fig. S6E). The concentration of ALP was 125 μg/L could completely hydrolyze PPi (Fig. S6F).

3.6. Performance of glyphosate detection

Using glyphosate as a classic model for OPs. The linear range and limit of detection of glyphosate were investigated under the optimal experimental conditions to demonstrate the performance of the constructed sensor for glyphosate. As shown in Fig. 4A, with increased concentration of glyphosate, higher fluorescence intensity at 440 nm and lower fluorescence intensity at 570 nm were observed, and leading

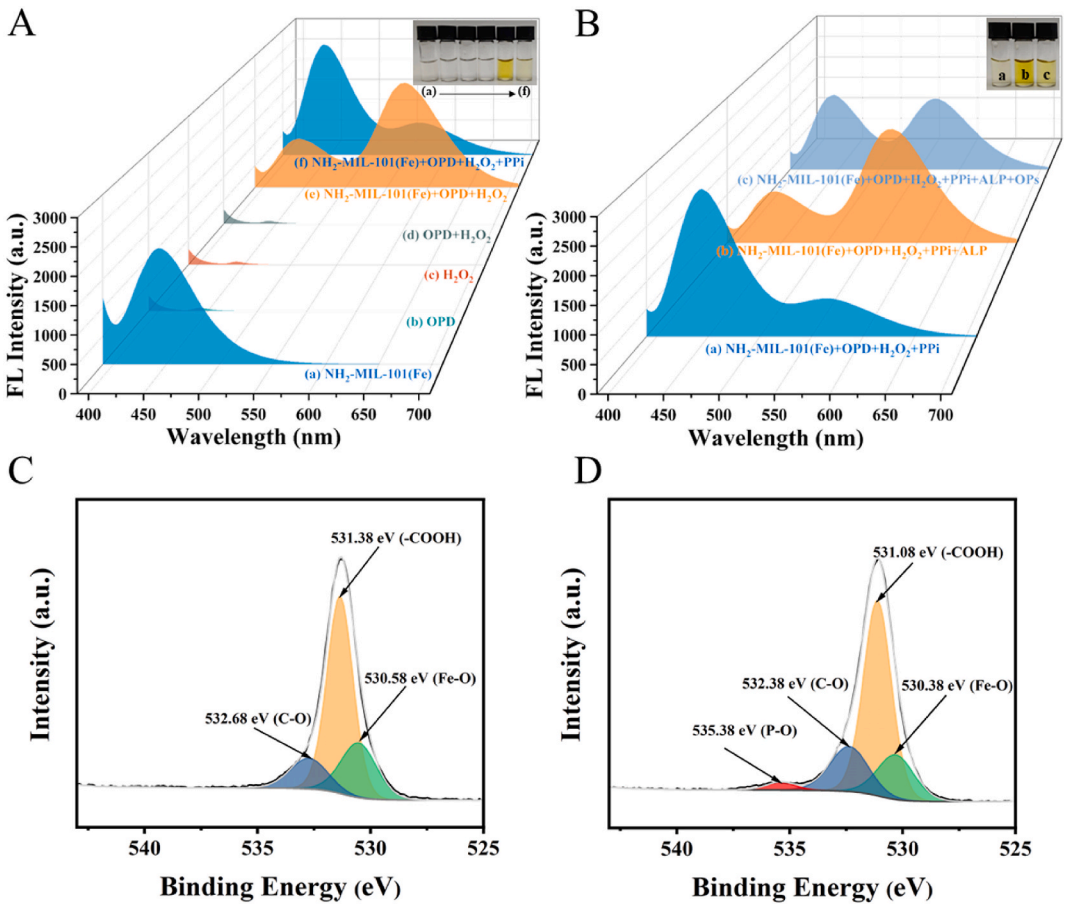

Fig. 3. (A, B) Fluorescence spectra of different systems in 0.1 M acetate buffer at pH 5.0. (C, D) The narrow range O 1s XPS spectra of the NH_2-MIL-101(Fe) before and after the addition of PPi.

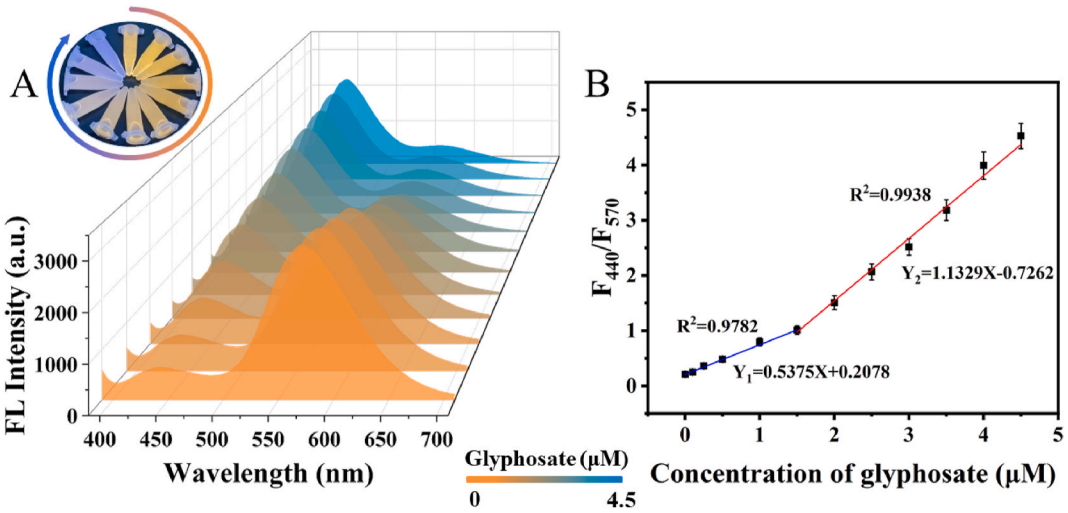

Fig. 4. (A) The fluorescence spectra of the constructed sensor in the presence of varying concentrations of glyphosate from 0 to 4.5 μM. Inset showed the corresponding photographs of sensing system under a 365 nm UV lamp. (B) Linear relationship between the F_{440}/F_{570} and different concentrations of glyphosate (0, 0.1, 0.25, 0.5, 1, 1.5, 2, 2.5, 3, 3.5, 4 and 4.5 μM).

to the fluorescence of sensing system color gradually changed from yellow to blue under a 365 nm UV lamp. The two-segment piecewise linear relationship between the F_{440}/F_{570} values and the concentration of glyphosate was observed (Fig. 4B).

The OPs could exert irreversible inhibitory effect on ALP, the ALP activity significantly decreased with the increasing concentration of the OPs, while the rate of decrease of ALP activity gradually slowed down. Hence, the increasing rate of F_{440} in the lower concentrations of OPs part was significantly faster than the higher concentrations of OPs when using a single fluorescence signal to detect OPs. Similarly, the decreasing rate of the lower concentrations of OPs part was significantly faster than the higher concentrations of OPs (Fig. S7). In addition, due to the

numerical calculations were performed, which led to the linear relationship between the value of F_{440}/F_{570} and the concentration of OPs changed again. The above reasons resulted in the concentration of glyphosate has two-segment linear relationship with F_{440}/F_{570}. The linear equations could be expressed to $F_{440}/F_{570} = 0.5375X+0.2078$ ($R^2 = 0.9782$, X was the concentration of glyphosate) and $F_{440}/F_{570} = 1.1329X-0.7262$ ($R^2 = 0.9938$) in the dynamic ranges of 0–4.5 μM. The detection limit of this assay was 18.7 nM.

To verify the universality of method for detection of OPs, several types of common OPs were detected by the proposed method. As shown in Fig. S8, the two-segment linear relationships between the F_{440}/F_{570} values and the concentration of chlorpyrifos, dipterex and dimethoate were observed, the detection limits of 0.20 μM, 0.21 μM and 0.34 μM were obtained, respectively. All above the detection limit of glyphosate, indicating that glyphosate has strongest inhibitory effect on ALP under the same concentration. This was due to the different chemical structures of these OPs, resulting in their differences in the ability to bind and inhibit ALP.

To explore potential reasons for the observed differences, ALP was docked with different OPs using Autodock software, the images were visualized with the PyMOL software. It can be clearly seen that glyphosate (yellow parts) stably bond to Asp-Ser-Ala tripeptide sequences (green parts) in the active center region of ALP through the formation of hydrogen bonds (Fig. 5A), thereby inhibiting the activity of ALP [42]. To gain more insight into the binding state, the molecular docking results were analyzed using the online website proteins. plus. The carboxyl group of glyphosate was chelated with the catalytic metal atom Mg^{2+} in the active site of ALP, the phosphate ester structure produced interactions with Lys and Arg by forming the hydrogen bond and ionic interaction, respectively. The amino part interacted with Asp by ionic interaction (Fig. 5B).

According to the best energy ranking of different molecular docking results, the most stable conformation was selected. The relevant parameters were shown in Table S1, all OPs were able to inhibit the activity of ALP, the binding free energy and inhibitor constant of glyphosate were both the lowest, which indicated glyphosate has strongest ability to bind and inhibit ALP [43], the simulation results agreed well with the experimental results.

As shown in Fig. 6A, 8 kinds of common co-existing ions (Na^+, K^+, Mg+, Ca^{2+}, SO_4^{2-}, Cl^-, NO_3^-, CO_3^{2-}, and SO_4^{2-}) were used to study the detection selectivity of the ratiometric fluorescence sensor, the influence of these ions on the selectivity of glyphosate detection was negligible. The potential other types of pesticides (Imidacloprid, dinotefuran, thiamethoxam and carbendazim) and common compounds (Oxalic acid, glucose, citric acid) in fruit and vegetable were also tested (Fig. 6B), these compounds did not perturb detection of sensor. This good selectivity can be explained from two aspects: on the one hand, the activity of ALP could be specifically inhibited by OPs with phosphate ester structure, and on the other hand, the ratiometric fluorescence sensing mode could provide built-in calibration for eliminating external interference. The results indicated that constructed ratiometric fluorescence sensor has satisfactory selectivity for detection of OPs.

To further highlight the characteristics of constructed sensor, which was compared with previously reported typical glyphosate detection methods [44–48]. As shown in Table S2, the fluorescence sensing method for OPs generally relied on fluorescence signals with single or double emission peaks. However, the majority of the studies focused on finding two fluorescent materials with different emission peaks and utilizing a certain response mechanism to detect glyphosate in the construction strategy of ratiometric fluorescence sensor. In this study, only one material was used, NH_2-MIL-101(Fe) not only as fluorescent indicator but also as a catalyst for fluorescent substrates. In this way, additional steps in the synthesis of sensing materials were saved and variables caused by additional sensing materials were eliminated, making the detection results more accurate. In addition, this method had a wide linear range and low limit of detection, which could meet the demand for detection in the most food and environment samples.

3.7. Detection of real samples

To further verify practical feasibility of constructed fluorescence sensor, detection of glyphosate in real samples was investigated. As shown in Table 1, the recoveries of glyphosate in real samples were from 92.4 % to 115.6 %, the relative standard deviations were from 1.0 % to 12.1 %. All these results displayed relative recovery rate and acceptable standard deviation, indicating that the constructed ratiometric fluorescence sensor possessed good accuracy and precision in practical applications.

4. Conclusion

In summary, a ratiometric fluorescence sensor was constructed for sensitive detection of OPs based on multifunctional Fe-based MOF. The fluorescence of NH_2-MIL-101(Fe) was quenched by its catalytic product DAP, the quenching mechanism was FRET, and was accompanied by IFE. PPi bound to the surface of NH_2-MIL-101(Fe) through hydrogen bond interaction, and then chelated with metal center (Fe^{3+} or Fe^{2+}) in Fe-based MOF, thereby hindering electron transfer between Fe^{3+}/Fe^{2+} redox couple and causing a significant decrease of peroxidase-like activity. The inhibition mechanism of different OPs for ALP was discussed through molecular simulation, the binding patterns of OPs to the key amino acids in active center of ALP were indicated. This work not only expanded application for Fe-based MOF materials as sensing probe, but also developed a promising method for detection of OPs in real samples.

CRediT authorship contribution statement

Cheng-Lin Yang: Writing – original draft, Validation, Methodology, Investigation, Conceptualization. **Li-Hong Yu:** Software, Methodology, Formal analysis. **Yue-Hong Pang:** Writing – review & editing,

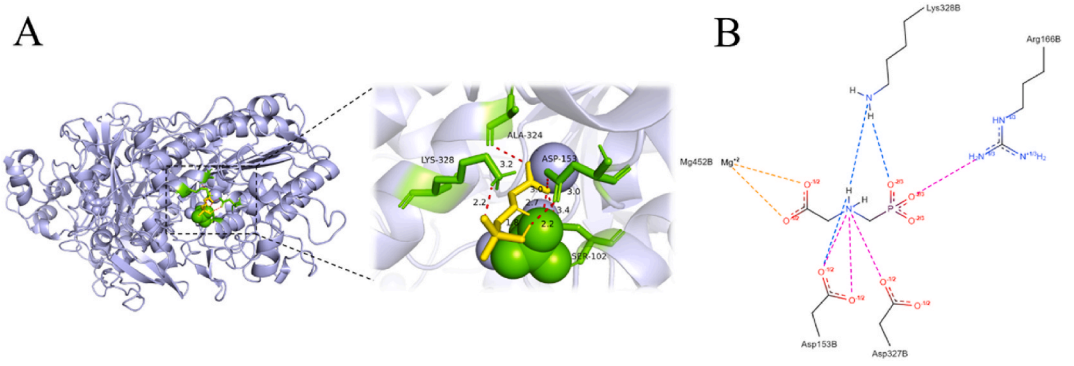

Fig. 5. (A) The 3D structure diagram of interaction between glyphosate and active area of ALP. (B) The 2D representation of stable conformation interaction.

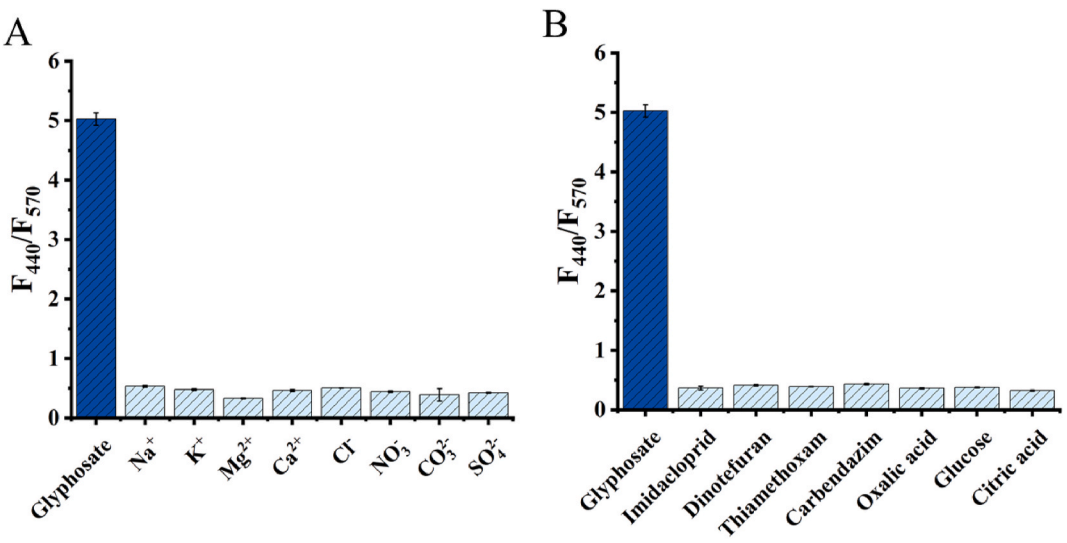

Fig. 6. (A) The selectivity of the constructed fluorescence sensor for detection glyphosate with the interferential substances include common cations and anions (10 μM each). (B) The selectivity of the constructed fluorescence sensor for detection glyphosate with the interferential substances include potential other types of pesticides and common compounds in fruit and vegetable (10 μM each).

Table 1
Determination of glyphosate in real samples (n = 3).

Samples	Added(μM)	Found(μM)	Recovery(%)	RSD(%)
	0	ND[1]	–	–
Tap water	0.5	0.54	108.2	11.6
	2.5	2.49	99.8	3.0
Lake water	0	ND	–	–
	0.5	0.58	115.6	12.1
	2.5	2.31	92.4	5.1
Soil	0	ND	–	–
	0.5	0.51	102.1	12.1
	2.5	2.37	94.8	2.8
	0	ND	–	–
Tea	0.5	0.56	112.9	6.8
	2.5	2.58	103.1	3.3
	0	2.65	–	1.0
Soybean	0.5	3.14	98.0	3.5
	2.5	4.98	93.2	1.8

ND[1]: Not detected.

Methodology, Formal analysis, Conceptualization. **Xiao-Fang Shen:** Supervision, Project administration, Funding acquisition.

Declaration of competing interest

The authors have no conflict of potential competing interest, financial or otherwise.

Data availability

Data will be made available on request.

Acknowledgments

This work was supported by the National Natural Science Foundation of China (22076067, 22276077).

Appendix ASupplementary data

Supplementary data to this article can be found online at https://doi.org/10.1016/j.talanta.2024.126516.

References

[1] Z. Li, J. Sun, L. Zhu, Organophosphorus pesticides in greenhouse and open-field soils across China: distribution characteristic, polluted pathway and health risk, Sci. Total Environ. 765 (2021) 142757, https://doi.org/10.1016/j.scitotenv.2020.142757.
[2] M. Zuo, Y. Yang, S. Jiang, C. Zhu, Y. Han, J. Hu, K. Ren, L. Cui, C.-Y. Zhang, Ultrathin-FeOOH-coated MnO2 nanozyme with enhanced catalase-like and oxidase-like activities for photoelectrochemical and colorimetric detection of organophosphorus pesticides, Food Chem. 445 (2024) 138716, https://doi.org/10.1016/j.foodchem.2024.138716.
[3] M. Zarei-Choghan, S. Jorfi, A. Saki, N. Jaafarzadeh, Spatial distribution, ecological and health risk assessment of organophosphorus pesticides identified in the water of Naseri artificial wetland, Iran, Mar. Pollut. Bull. 179 (2022) 113643, https://doi.org/10.1016/j.marpolbul.2022.113643.
[4] G. Wang, J. Li, N. Xue, A. Abdulkreem Al-Huqail, H.S. Majdi, E. Darvishmoghaddam, H. Assilzadeh, M.A. Khadimallah, H.E. Ali, Risk assessment of organophosphorus pesticide residues in drinking water resources: Statistical and Monte-Carlo approach, Chemosphere 307 (2022) 135632, https://doi.org/10.1016/j.chemosphere.2022.135632.
[5] S. Jullakan, O. Bunkoed, S. Pinsrithong, Solvent-assisted dispersive liquid-solid phase extraction of organophosphorus pesticides using a polypyrrole thin film–coated porous composite magnetic sorbent prior to their determination with GC-MS/MS, Microchim. Acta 187 (2020) 677, https://doi.org/10.1007/s00604-020-04649-1.
[6] J.I. Cacho, N. Campillo, P. Viñas, M. Hernández-Córdoba, In situ ionic liquid dispersive liquid-liquid microextraction coupled to gas chromatography-mass spectrometry for the determination of organophosphorus pesticides, J. Chromatogr. A 1559 (2018) 95–101, https://doi.org/10.1016/j.chroma.2017.12.059.
[7] L. Xu, X. Zhang, A.M. Abd El-Aty, Y. Wang, Z. Cao, H. Jia, J.P. Salvador, A. Hacimuftuoglu, X. Cui, Y. Zhang, K. Wang, Y. She, F. Jin, L. Zheng, B. Pujia, J. Wang, M. Jin, B.D. Hammock, A highly sensitive bio-barcode immunoassay for multi-residue detection of organophosphate pesticides based on fluorescence anti-quenching, J. Pharm. Anal. 12 (2022) 637–644, https://doi.org/10.1016/j.jpha.2022.05.004.
[8] L. Song, Q. Zhang, L. Min, X. Guo, W. Gao, L. Cui, C.-y. Zhang, Electrochemiluminescence enhanced by isolating ACQphores in imine-linked covalent organic framework for organophosphorus pesticide assay, Talanta 266 (2024) 124964, https://doi.org/10.1016/j.talanta.2023.124964.
[9] F. Tong, Z. Yang, Z. Wang, W. Liu, W. Jiang, L. Zhu, L. Wang, M. Zheng, R. Hou, Y. Zhou, Y. Liu, Enzyme-mediated Ru@UiO-66@MnO_2 NSs/thiamine-based ratiometric fluorescence sensor for visual detection of organophosphorus pesticide residues, Food Chem. 429 (2023) 136945, https://doi.org/10.1016/j.foodchem.2023.136945.
[10] F. Xu, X. Li, C. Chen, Z. Liang, G. Xu, F. Wei, J. Yang, Q. Hu, Y. Cen, A dual-emission ratiometric fluorescence strategy with enzyme-based inhibition for organophosphorus pesticides determination, Microchim. Acta 190 (2023) 337, https://doi.org/10.1007/s00604-023-05923-8.
[11] Z. Zhang, L. Zhang, P. Han, Q. Liu, A luminescent probe based on terbium-based metal–organic frameworks for organophosphorus pesticides detection, Microchim. Acta 189 (2022) 438, https://doi.org/10.1007/s00604-022-05508-x.
[12] Y. Yang, X. Lei, B. Liu, H. Liu, J. Chen, G. Fang, J. Liu, S. Wang, A ratiometric fluorescent sensor based on metalloenzyme mimics for detecting

organophosphorus pesticides, Sensor. Actuator. B Chem. 377 (2023) 133031, https://doi.org/10.1016/j.snb.2022.133031.
[13] K. Yang, P. Jia, J. Hou, S. Zhao, L. Wang, An ingenious turn-on ratiometric fluorescence sensor for sensitive and visual detection of tetracyclines, Food Chem. 396 (2022) 133693, https://doi.org/10.1016/j.foodchem.2022.133693.
[14] W. Xie, J. Liu, Y. Qu, F. Du, Construction of a ratiometric fluorescent sensing platform based on near-infrared carbon dots for organophosphorus pesticides detection, Anal. Sci. 39 (2023) 1097–1106, https://doi.org/10.1007/s44211-023-00319-3.
[15] X. Yan, H. Li, X. Han, X. Su, A ratiometric fluorescent quantum dots based biosensor for organophosphorus pesticides detection by inner-filter effect, Biosens. Bioelectron. 74 (2015) 277–283, https://doi.org/10.1016/j.bios.2015.06.020.
[16] Q. Yang, J. Wang, X. Chen, W. Yang, H. Pei, N. Hu, Z. Li, Y. Suo, T. Li, J. Wang, The simultaneous detection and removal of organophosphorus pesticides by a novel Zr-MOF based smart adsorbent, J. Mater. Chem. A 6 (2018) 2184–2192, https://doi.org/10.1039/c7ta08399hrsc.li/materials-a.
[17] S. Farhadi, A. Riahi-Madvar, G. Sargazi, M. Mortazavi, Immobilization of Lepidium draba peroxidase on a novel Zn-MOF nanostructure, Int. J. Biol. Macromol. 173 (2021) 366–378, https://doi.org/10.1016/j.ijbiomac.2020.12.216.
[18] D. Li, S. Zhang, X. Feng, H. Yang, F. Nie, W. Zhang, A novel peroxidase mimetic Co-MOF enhanced luminol chemiluminescence and its application in glucose sensing, Sensor. Actuator. B Chem. 296 (2019) 126631, https://doi.org/10.1016/j.snb.2019.126631.
[19] F. Ghourchian, N. Motakef-Kazemi, E. Ghasemi, H. Ziyadi, Zn-based MOF-chitosan-Fe_3O_4 nanocomposite as an effective nano-catalyst for azo dye degradation, J. Environ. Chem. Eng. 9 (2021) 106388, https://doi.org/10.1016/j.jece.2021.106388.
[20] X. Yu, Y. Wei, W. Qi, M. Wang, Catalytic metal–organic framework-melamine foam composite as an efficient material for the elimination of organic pollutants, Environ. Sci. Pollut. Res. 30 (2023) 44266–44275, https://doi.org/10.1007/s11356-023-25441-7.
[21] R. Du, Y. Wu, Y. Yang, T. Zhai, T. Zhou, Q. Shang, L. Zhu, C. Shang, Z. Guo, Porosity engineering of MOF-based materials for electrochemical energy storage, Adv. Energy Mater. 11 (2021) 2100154, https://doi.org/10.1021/acsami.8b04737.
[22] N.A.A. Qasem, R. Ben-Mansour, M.A. Habib, An efficient CO_2 adsorptive storage using MOF-5 and MOF-177, App, At. Energ. 210 (2018) 317–326, https://doi.org/10.1016/j.apenergy.2017.11.011.
[23] L. Yuan, Z. Gan, Y. Fan, F. Ding, X. Xu, X. Chen, X. Zou, W. Zhang, Thermal-controlled active sensor module using enzyme-regulated UiO-66-NH_2/MnO_2 fluorescence probe for total organophosphorus pesticide determination, J. Hazard Mater. 436 (2022) 129111, https://doi.org/10.1016/j.jhazmat.2022.129111.
[24] L. Wang, Z. Hu, S. Wu, J. Pan, X. Xu, X. Niu, A peroxidase-mimicking Zr-based MOF colorimetric sensing array to quantify and discriminate phosphorylated proteins, Anal. Chim. Acta 1121 (2020) 26–34, https://doi.org/10.1016/j.aca.2020.04.073.
[25] P. Liu, X. Li, X. Xu, K. Ye, L. Wang, H. Zhu, M. Wang, X. Niu, Integrating peroxidase-mimicking activity with photoluminescence into one framework structure for high-performance ratiometric fluorescent pesticide sensing, Sensor. Actuator. B Chem. 328 (2021) 129024, https://doi.org/10.1016/j.snb.2020.129024.
[26] S. Li, X. Hu, Q. Chen, X. Zhang, H. Chai, Y. Huang, Introducing multifunctional metal-organic frameworks to the construction of a novel ratiometric fluorescence sensor for screening acid phosphatase activity, Biosens. Bioelectron. 137 (2019) 133–139, https://doi.org/10.1016/j.bios.2019.05.010.
[27] J. Song, M. Huang, X. Lin, S.F.Y. Li, N. Jiang, Y. Liu, H. Guo, Y. Li, Novel Fe-based metal–organic framework (MOF) modified carbon nanofiber as a highly selective and sensitive electrochemical sensor for tetracycline detection, Chem. Eng. J. 427 (2022) 130913, https://doi.org/10.1016/j.cej.2021.130913.
[28] Y. Xing, H. Si, D. Sun, X. Hou, Magnetic Fe_3O_4@NH_2-MIL-101(Fe) nanocomposites with peroxidase-like activity for colorimetric detection of glucose, Microchem. J. 156 (2020) 104929, https://doi.org/10.1016/j.microc.2020.104929.
[29] Y. Zhang, Z. Zhang, Z. Wang, H. Pan, Y. Lin, D. Chang, Sensitive detection of prostate-specific antigen based on dual signal amplification of Fc@MgAl-LDH and NH_2-MIL-101(Fe), Biosens. Bioelectron. 190 (2021) 113437, https://doi.org/10.1016/j.bios.2021.113437.
[30] C. Lou, F. Yang, L. Zhu, Q. Sun, Y. Yang, J. Guo, Dual-function sensor based on NH2-MIL-101(Fe)@Cu/CeO_2 nanozyme for colorimetric and fluorescence detection of heavy metals, Colloid. Surface. 677 (2023) 132398, https://doi.org/10.1016/j.colsurfa.2023.132398.
[31] Y. Chen, K. Tang, X. Wang, Q. Zhou, S. Tang, X. Wu, P. Zhao, H. Lei, Z. Yang, Z. Zhang, A homogeneous capillary fluorescence imprinted nanozyme intelligent sensing platform for high sensitivity and visual detection of triclocarban, Sensor. Actuator. B Chem. 382 (2023) 133543, https://doi.org/10.1016/j.snb.2023.133543.
[32] C.-Q. Wan, Y.-H. Pang, Y.-W. Feng, X.-F. Shen, A ratio fluorescence sensor based on rhodamine B embedded metal-organic framework for glyphosate detection in agri-food products, Food Chem. 394 (2022) 133446, https://doi.org/10.1016/j.foodchem.2022.133446.
[33] H. Yi, J. Ran, Y. Tan, Z. Wang, B. Liu, A colorimetric/electrochemical sensor based on coral-like $CuCo_2O_4$@AuNPs composites for sensitive dopamine detection, Anal. Bioanal. Chem. (2023), https://doi.org/10.1007/s00216-023-05014-w.
[34] W. Duan, J. Wang, X. Peng, S. Cao, J. Shang, Z. Qiu, X. Lu, J. Zeng, Rational design of trimetallic AgPt–Fe_3O_4 nanozyme for catalyst poisoning-mediated CO colorimetric detection, Biosens. Bioelectron. 223 (2023) 115022, https://doi.org/10.1016/j.bios.2022.115022.
[35] J. Xiao, F. Shi, Y. Zhang, M. Peng, J. Xu, J. Li, Z. Chen, Z. Yang, A MOF nanozyme-mediated acetylcholinesterase-free colorimetric strategy for direct detection of organophosphorus pesticides, Chem. Commun. 60 (2024) 996–999, https://doi.org/10.1039/d3cc05381drsc.li/chemcomm.
[36] X. Yue, Y. Li, S. Xu, J. Li, M. Li, L. Jiang, M. Jie, Y. Bai, A portable smartphone-assisted ratiometric fluorescence sensor for intelligent and visual detection of malachite green, Food Chem. 371 (2022) 131164, https://doi.org/10.1016/j.foodchem.2021.131164.
[37] H. Tan, X. Wu, Y. Weng, Y. Lu, Z.-Z. Huang, Self-assembled FRET nanoprobe with metal–organic framework as a scaffold for ratiometric detection of hypochlorous acid, Anal. Chem. 92 (2020) 3447–3454, https://doi.org/10.1021/acs.analchem.9b05565.
[38] W. Shi, T. Li, N. Chu, X. Liu, M. He, B. Bui, M. Chen, W. Chen, Nano-octahedral bimetallic Fe/Eu-MOF preparation and dual model sensing of serum alkaline phosphatase (ALP) based on its peroxidase-like property and fluorescence, Mat. Sci. Eng. C-mater. 129 (2021) 112404, https://doi.org/10.1016/j.msec.2021.112404.
[39] K. Huang, Y. Zhuang, Z. Wang, L. Ou, J. Cen, S. Lu, Y. Qi, Bioavailability of organic phosphorus compounds to the harmful dinoflagellate karenia mikimotoi, Microorganisms 9 (2021) 1961, https://doi.org/10.3390/microorganisms9091961.
[40] W. Dong, G. Chen, X. Hu, X. Zhang, W. Shi, Z. Fu, Molybdenum disulfides nanoflowers anchoring iron-based metal organic framework: a synergetic catalyst with superior peroxidase-mimicking activity for biosensing, Sensor. Actuator. B Chem. 305 (2020) 127530, https://doi.org/10.1016/j.snb.2019.127530.
[41] K. Ye, L. Wang, H. Song, X. Li, X. Niu, Multifunctional MIL-53(Fe) with pyrophosphate-mediated peroxidase-like activity and oxidation-stimulated fluorescence switching for alkaline phosphatase detection, J. Mater. Chem. B 7 (2019) 4794–4800, https://doi.org/10.1039/c9tb00951ersc.li/materials-b.
[42] Z. Yan, Z. Peng, J. Lai, P. Xu, P. Qiu, Simplifying the complexity: single enzyme (choline oxidase) inhibition-based biosensor with dual-readout method for organophosphorus pesticide detection, Talanta 265 (2023) 124905, https://doi.org/10.1016/j.talanta.2023.124905.
[43] Y.-H. Chu, Y. Li, Y.-T. Wang, B. Li, Y.-H. Zhang, Investigation of interaction modes involved in alkaline phosphatase and organophosphorus pesticides via molecular simulations, Food Chem. 254 (2018) 80–86, https://doi.org/10.1016/j.foodchem.2018.01.187.
[44] X.-Y. Xu, B. Yan, X. Lian, Wearable glove sensor for non-invasive organophosphorus pesticide detection based on a double-signal fluorescence strategy, Nanoscale 10 (2018) 13722–13729, https://doi.org/10.1039/c8nr03352hrsc.li/nanoscale.
[45] S. Liu, S.G. Liu, W. Jiang, Q. Zhao, W. Gao, X. Shi, Detection of organophosphorus pesticides using silver-coated gold nanoparticles, ACS Appl. Nano Mater. 5 (2022) 16402–16412, https://doi.org/10.1021/acsanm.2c03478.
[46] J. Jiménez-López, E.J. Llorent-Martínez, P. Ortega-Barrales, A. Ruiz-Medina, Graphene quantum dots-silver nanoparticles as a novel sensitive and selective luminescence probe for the detection of glyphosate in food samples, Talanta 207 (2020) 120344, https://doi.org/10.1016/j.talanta.2019.120344.
[47] X. Tong, G. Cai, L. Xie, T. Wang, Y. Zhu, Y. Peng, C. Tong, S. Shi, Y. Guo, Threaded 3D microfluidic paper analytical device-based ratiometric fluorescent sensor for background-free and visual detection of organophosphorus pesticides, Biosens. Bioelectron. 222 (2023) 114981, https://doi.org/10.1016/j.bios.2022.114981.
[48] H. Wang, X. Liu, X. Wang, P. Qiu, P. Li, Enzyme-free ratiometric fluorescence and colorimetric dual-signal determination of glyphosate based on copper nanoclusters (ZIF/CuNCs) combined with blue carbon dots (bCDs), Spectrochim. Acta 308 (2024) 123796, https://doi.org/10.1016/j.saa.2023.123796.